Shape Analysis of Brain Structures Using Physical and Experimental Modes

John Martin, Alex Pentland, and Ron Kikinis

Surgical Planning Laboratory, Department of Radiology
Brigham and Women's Hospital
75 Francis Street, Boston, MA 02115

Perceptual Computing Group, The Media Laboratory
Massachusetts Institute of Technology
20 Ames Street, Cambridge, MA 02139

1 Introduction

Various neurological disorders affect the gross anatomical shape of different brain structures. Hydrocephalus, for example, affects the morphology of the ventricular system. These changes have been studied for several decades, using both postmortem and in vivo methods. Recent advances in the contrast and resolution of magnetic resonance (MR) scanners now make it possible to study these shape effects in vivo and noninvasively, with the potential for better diagnosis and treatment. Our aim is to quantitatively describe these pathological shape deformations.

Because of both genetic and environmental factors, however, biological structures have a large normal range of variation. The onset of a disease introduces further changes in morphology, with each particular disease causing its own type of shape changes and range of variation in these changes. Therefore to properly study the pathological deformations, we must first account for the large normal variation in biological shape.

For structures inside the cranium, part of this normal shape variability is due to the different head shapes seen across individuals. These macroscopic shape effects interfere with the analysis of local shape deformations caused by disease.

What is needed then is a method that separates out these two types of deformations, allowing just the disease deformations to be analyzed. In this paper we create a mathematical framework that (1) separates out disease deformation from head shape deformation, and (2) allows us to represent the deformations caused by disease in an intuitive manner. This is accomplished by using the finite element method (FEM) to create a physical model that describes the macroscopic effects caused by different head shapes. After elastically warping the cranial contents according to this physical model, we are left with residual shape differences across patients that are largely independent of head shape. Because detailed physical models of neurological diseases do not exist, we turn to statistical techniques to examine this data.

We have selected the ventricles of the brain to study disease and head shape deformations. Figure 1 shows the ventricles of a healthy volunteer, a patient with Alzheimer's disease (AD), and a patient with normal-pressure hydrocephalus (NPH). Both of the disorders cause the ventricles to enlarge, but in different amounts and in different ways.

Figure 1: Reconstructions of the ventricular system of the human brain created from MR images.
Top: Normal, healthy adult.
Bottom Left: Alzheimer's disease causes an enlargement of ventricles.
Bottom Right: Normal-pressure hydrocephalus causes an even greater enlargement of the ventricles, along with an overall "puffy" appearance.

2 Related Work

Terzopoulus *et al.* [7] used a physical model with a very large number of degrees of freedom to perform dynamic shape fitting. Pentland and Sclaroff [5] employed a much smaller number of degrees of freedom, representing shape in terms of an object's physical deformation modes. Instead of using the modes of a particular object, Bookstein [1] described shape deformation in terms of the physical deformation modes of an infinite thin plate, applying it primarily in the biological domain. Collins *et al.* [2] used this thin plate model to calculate brain deformation. This deformation was then applied to internal structures of a pre-defined anatomical atlas in order to improve segmentation.

Instead of physically modeling the structure under study, researchers have also sought to approximate the modes of variation through experimental observation. Cootes *et al.* [3] used principal component analysis to experimentally describe the modes of variation inherent in a training set of 2D heart images. Hill *et al.* [4] extended this technique to 3D and analyzed the ventricles of the brain for purposes of segmentation and representation.

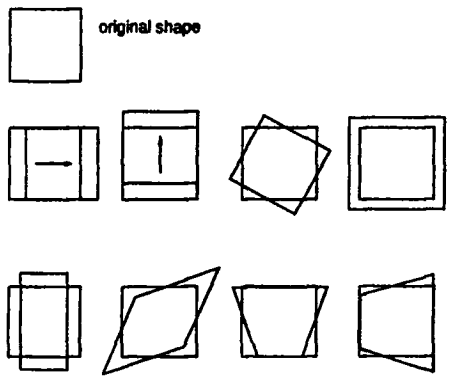

Figure 2: Physical modes of a square.

)ur method differs from the above work in the fol-
ing respects. First, all of the above techniques use
ier physical modeling or experimental observation in
er to represent shape deformation. In our method,
combine *both* physical and experimental techniques
)rder to describe shape variation. Second, in addi-
ı to representing the modes of variation in healthy
in structures, we also investigate the modes of vari-
)n caused by different disease processes. Finally, we
these modes to classify patients into different dis-
ɜ categories.

3 Deformation Model

Physical Modes

ng the FEM, we can write the dynamics of an elastic
.y as

$$\mathbf{M}\ddot{\mathbf{U}} + \mathbf{C}\dot{\mathbf{U}} + \mathbf{K}\mathbf{U} = \mathbf{R} \tag{1}$$

:re $\mathbf{M}$ is the mass matrix, $\mathbf{C}$ is a damping matrix, $\mathbf{K}$
ıe stiffness matrix, $\mathbf{U}$ is a vector of nodal displace-
ıts, and $\mathbf{R}$ is a vector of nodal forces being exter-
y applied to the system. The equilibrium solution
)quation 1 is

$$\mathbf{K}\mathbf{U} = \mathbf{R}. \tag{2}$$

he technique of modal analysis consists of comput-
the eigenvectors of $\mathbf{K}$ by applying an orthogonal
ısform to Equation 1. These eigenvectors are called
free vibration modes of the physical system. Any
trary displacement of the nodes can be written as
ıear combination of these physical modes:

$$\mathbf{U} = \mathbf{\Phi}\mathbf{a} = \sum_{i=1}^{3N} \mathbf{\Phi}_i a_i, \tag{3}$$

re N is the number of nodes.
his is illustrated by the two-dimensional example
vn in Figure 2. By placing one node at each cor-
of the square and assigning material properties, a
ıess matrix $\mathbf{K}$ can be constructed. Next, the modal
sformation is applied to the system. The resulting
t free vibration modes (the eigenvectors of $\mathbf{K}$) are
vn in the figure.

3.2 Experimental Modes

Instead of modeling the system as an elastic material, we can instead assume nothing about it and just collect data samples of the displacements of each node. Here each node is treated as a random variable, and after collecting P samples of deformed objects, we can form the sample covariance matrix of these measurements:

$$\mathbf{S} = \frac{1}{P-1}\sum_{p=1}^{P}(\mathbf{U} - \overline{\mathbf{U}})(\mathbf{U} - \overline{\mathbf{U}})^T. \tag{4}$$

Diagonalizing $\mathbf{S}$ by performing a principal component analysis gives the experimental modes of variation, which we assemble as the columns in a matrix $\mathbf{\Psi}$. Any arbitrary displacement of the nodes can now be written as a linear combination of these experimental modes:

$$\mathbf{U} = \mathbf{\Psi}\mathbf{b} = \sum_{i=1}^{3N} \mathbf{\Psi}_i b_i. \tag{5}$$

3.3 The Connection

The connection between physical and experimental modes comes through the close relationship between mechanical and probabilistic prior models[6]. The mechanical viewpoint is the one we have used above, modeling the elastic field by a stiffness matrix $\mathbf{K}$. We can instead interpret Equation 2 and its solution

$$\mathbf{U} = \mathbf{K}^{-1}\mathbf{R} \tag{6}$$

from a probabilistic viewpoint, by treating $\mathbf{U}$ and $\mathbf{R}$ as random vectors related by the linear transform $\mathbf{K}^{-1}$. By assuming that the elements of $\mathbf{R}$ are independent and isotropic, the following relationship can be derived:

$$\mathbf{S} \approx \mathbf{K}^{-1}\mathbf{K}^{-1}. \tag{7}$$

This relates the sample covariance matrix obtained through experimentation to the stiffness matrix obtained through modeling.

Because of Equation 7, the orthogonal transform from Section 3.1 that diagonalized $\mathbf{K}$ will also diagonalize $\mathbf{S}$. Therefore the eigenvectors of $\mathbf{S}$ and $\mathbf{K}$ are identical, which says that physical and experimental modes are the same. In other words, the directions of variability in a set of data found by diagonalizing the sample covariance matrix are precisely the free vibration modes of the system.

Assume that the deformation in a system is caused by two independent processes. Furthermore, assume that one of the processes can be modeled physically, and that the other cannot, but is amenable to experimental observation. Then the total deformation can be written as the sum of the deformations caused by each process:

$$\mathbf{U} = \mathbf{U}^P + \mathbf{U}^E. \tag{8}$$

Using Equations 3 and 5, we can write the total deformation in terms of the physical modes of the first process and the experimental modes of the second process:

$$\mathbf{U} = \mathbf{U}^P + \mathbf{U}^E = \mathbf{\Phi}\mathbf{a} + \mathbf{\Psi}\mathbf{b}. \tag{9}$$

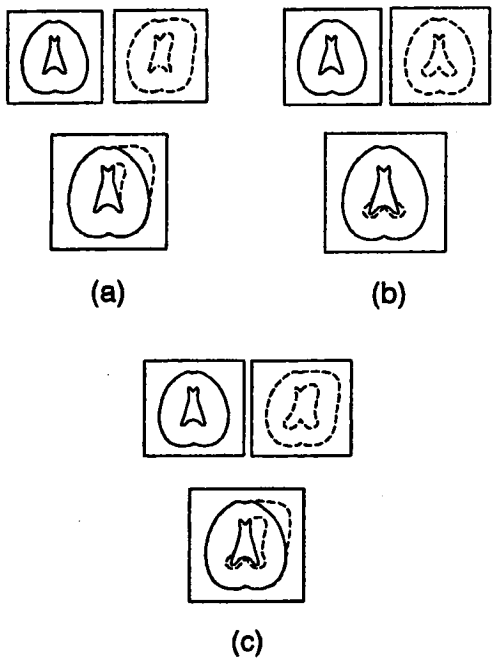

Figure 3: Schematic representation of ICC and ventricles. (a) Different shaped ICCs, no ventricular disease present. The only ventricular shape difference is due to the ICC shape difference. (b) Same shaped ICCs, with ventricular disease. The lower tips of the ventricles are expanded due to the disease. This shape difference is not caused by different ICC shapes. (c) Different shaped ICCs, with ventricular disease. The pathological difference in ventricular shape is partially masked out by the nonpathological difference due to ICC shape.

4 Ventricular Deformation

We want to be able to classify the ventricle shapes as either normal, or as belonging to one of several known disease classes. Each disease affects the shape of the ventricles in a unique way, and it is this shape difference that we want to use to do the classification. Unfortunately ventricular shape is also affected by overall head shape, which has nothing to do with the disease processes. This is illustrated in Figure 3, which shows schematic drawings of the intra-cranial cavity (ICC) and the ventricles, in various configurations.

We can compute the ventricular deformations caused by different ICC shapes by modeling the brain as a homogeneous piece of elastic material. This model is discretized by assuming the mass to be concentrated at M nodes. A stiffness matrix $\mathbf{K}$ is then formed using the assigned material properties and the geometry of the nodes. The nodes are chosen in such a way that they are independent of any pathological effects. This procedure enables us to express ventricular deformation in terms of the physical modes of the ICC.

Because the physical processes underlying most diseases are poorly understood, we have no hope of creating even a rough physical model of the ventricular deformation due to pathology. We therefore turn to observation, and represent the pathological ventricular deformation by the experimental modes of variation.

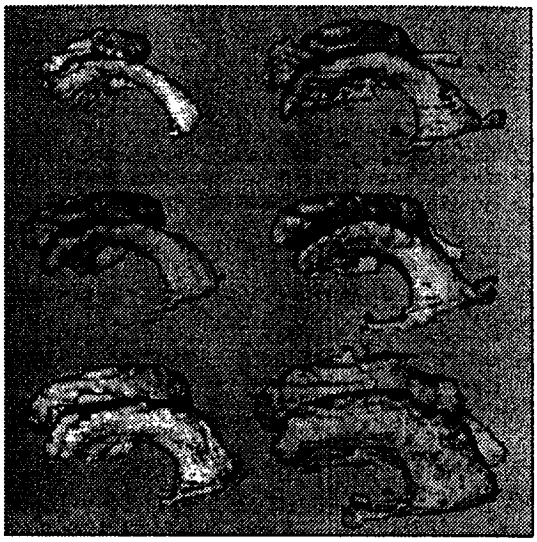

Figure 4: Ventricular deformation modes.

We can therefore represent the overall ventricular deformation using a modified version of Equation 9:

$$\mathbf{U} = \mathbf{U}^P + \mathbf{U}^E = \mathbf{H}\Phi\mathbf{a} + \Psi\mathbf{b} \qquad (10)$$

where $\mathbf{H}$ is the matrix of FEM interpolation functions from the physical model of the ICC.

5 Modes of Variation

We applied our method to twenty-five patients (9 with AD, 7 with NPH, and 9 normals). Figure 4 illustrates some of the ventricular modes of variation obtained. The top left shows the average ventricular system obtained from the normal volunteers, while the first mode of variation among the normals is shown in the top right. This mode shows that overall ventricular volume and length, as well as the size of the posterior horns, are important features in discriminating among normal ventricles.

The middle row consists of the average AD ventricular system along with the first AD mode of variation. Some enlargement in the average AD is seen relative to the average normal. Similar to the normals, the first AD mode indicates that the size of the posterior horns is important. The size of the inferior horns also appears to be significant.

The bottom row shows the average and first mode of variation for NPH. The most important features are the large expansion and an overall "puffy" shape.

6 Experiments and Results

The first two rows of Table 1 show the results of running a gaussian quadratic classifier on the experimental modes of the ventricle data. As a benchmark, the

Feature(s)	# Correct
Experimental Modes (with warping)	25
xperimental Modes (without warping)	24
Ratio of ventricular to ICC volume	20
Ventricular volume	22

Table 1: Number of patients correctly classified.

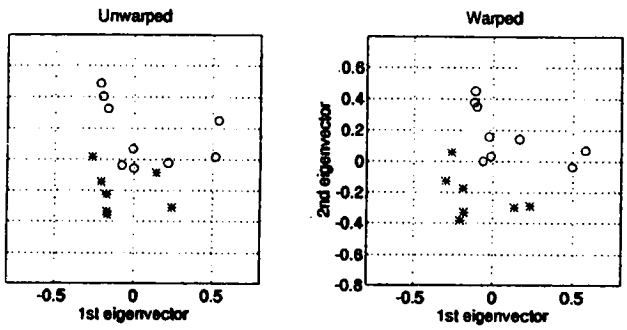

ure 5: Projection onto the top two eigenvectors com-
ed from normals and NPH patients. The o's are
lthy volunteers, and the *'s are patients with NPH.

two rows show the classification results when using
:h simpler features, either just ventricular volume
entricular volume normalized by a patient's overall
volume. We see that the experimental modes cal-
ıted after discounting for the ICC's physical modes
vide the best discriminatory features. To test the
ıstness of this result, we varied the number of eigen-
:ors used in the classification, as well as the type of
sifier. In almost all of the cases the best results were
ıined when using the physically-discounted experi-
ıtal modes as features.

ince the results in Table 1 represent effects taking
e in many dimensions, they are hard to visualize.
therefore took just the normal volunteers and the
H patients, and performed an eigenanalysis both
ı and without first warping based on the ICCs. The
ections onto just the top two eigenvectors are shown
igure 5. An improvement in class separability can
een when warping with the physical modes of the
s.

7 Summary

have presented a new method that describes shape
rmation by using both physical modeling and sta-
cal techniques. When applied to the human brain,
method is able to separate out pathological shape
rmation from normal shape deformation, allowing
er representation and analysis of the deformations
to disease. The representation is in the form of a disease's deformation modes, which provide a very natural basis set in which to examine pathological shape deformation. The analysis suggests that by first discounting the experimental modes of a brain structure by the physical modes of the intra-cranial cavity, it may be possible to improve disease classification.

In summary, there are three main contributions of this work. First, we have suggested a shape representation method for brain structures that we believe to be intuitive, in the sense that it can be thought of as a more sophisticated version of the simpler idea of using volume and head size to describe and normalize the shape of a brain structure. Second, by using the connection between physically-based modeling and probability, we have put our method into a consistent mathematical framework. This enabled us to decouple the modes of variation caused by different physical processes, and to use these decoupled modes in standard pattern recognition algorithms. Third, by applying our method to medical data, we have indicated that it may possible to improve disease classification by discounting the experimental modes with the physical modes associated with head shape. These experimental modes were displayed as an illustration of the ventricular deformation modes caused by Alzheimer's disease and by normal-pressure hydrocephalus.

Acknowledgments

The authors would like to thank Stan Sclaroff and Irfan Essa their helpful advice, and Mike Matsumae for providing the MR brain data.

References

[1] F. L. Bookstein. *Morphometric Tools for Landmark Data: Geometry and Biology.* Cambridge University Press, 1991.

[2] D. L. Collins, T. M. Peters, W. Dai, and A. C. Evans. Model based segmentation of individual brain structures from MRI data. In *SPIE: Visualization in Biomedical Computing*, pages 10–23, 1992.

[3] T.F. Cootes, D. H. Cooper, C. J. Taylor, and J. Graham. Trainable method of parametric shape description. *Image and Vision Computing*, 10(5):289–294, June 1992.

[4] A. Hill, T. F. Cootes, and C.J. Taylor. A generic system for image interpretation using flexible templates. In *Proc. British Machine Vision Conference*, pages 276–285, 1992.

[5] A. P. Pentland and S. Sclaroff. Closed-form solutions for physically based shape modeling and recognition. *IEEE Trans. Pattern Anal. Machine Intell.*, 13(7):715–729, July 1991.

[6] R. Szeliski. *Bayesian Modeling of Uncertainty in Low-level Vision.* Kluwer Academic Publishers, 1989.

[7] D. Terzopoulos, A. Witkin, and M. Kass. Symmetry-seeking models and 3D object reconstruction. *Int. J. Comput. Vision*, 1:211–221, 1987.